

LD-EnSF: Synergizing Latent Dynamics with Ensemble Score Filters for Fast Data Assimilation with Sparse Observations

Pengpeng Xiao^{1,2}, Phillip Si¹, and Peng Chen^{1, *}

¹School of Computational Science and Engineering, Georgia Institute of Technology, Atlanta, GA 30308, USA

²Department of Physics, Fudan University, Shanghai 200437, China

*Corresponding author. Email: pchen402@gatech.edu

Abstract

Data assimilation techniques are crucial for correcting the trajectory when modeling complex physical systems. A recently developed data assimilation method, Latent Ensemble Score Filter (Latent-EnSF), has shown great promise in addressing the key limitation of EnSF for highly sparse observations in high-dimensional and nonlinear data assimilation problems. It performs data assimilation in a latent space for encoded states and observations in every assimilation step, and requires costly full dynamics to be evolved in the original space. In this paper, we introduce Latent Dynamics EnSF (LD-EnSF), a novel methodology that completely avoids the full dynamics evolution and significantly accelerates the data assimilation process, which is especially valuable for complex dynamical problems that require fast data assimilation in real time. To accomplish this, we introduce a novel variant of Latent Dynamics Networks (LDNets) to effectively capture and preserve the system’s dynamics within a very low-dimensional latent space. Additionally, we propose a new method for encoding sparse observations into the latent space using Long Short-Term Memory (LSTM) networks, which leverage not only the current step’s observations, as in Latent-EnSF, but also all previous steps, thereby improving the accuracy and robustness of the observation encoding. We demonstrate the robustness, accuracy, and efficiency of the proposed method for two challenging dynamical systems with highly sparse (in both space and time) and noisy observations.

1 Introduction

Numerical methods for partial differential equations (PDEs), such as the finite element method, have established themselves as reliable tools for simulating complex scientific problems that lack closed-form solutions. However, these simulations are prone to errors arising from various sources, including parameter misspecification, model simplifications, numerical inaccuracies, and inherent uncertainties within the model. Without proper management, these errors can accumulate and propagate over time, ultimately leading to significant deviations from the true state. This challenge is particularly pronounced in real-world applications like weather forecasting [42], computational fluid dynamics [9], and sea ice modeling [47], where systems involve intricate interactions and substantial uncertainties. As a result, data assimilation techniques [41], which integrate additional observations at specific intervals to mitigate error accumulation, are becoming increasingly essential in modern simulation workflows.

1.1 A short review of data assimilation methods and our contributions

Various data assimilation methods have been developed to address the challenge of integrating observational data into model simulations. Traditional approaches, particularly those based on Bayesian filtering, have dominated this area due to their computational efficiency, leveraging the Markovian assumption on prior states. Examples include the Kalman Filter [23] and particle filters [26]. Building on these, the Ensemble Kalman Filter (EnKF)[17] and its variants [22, 7] were developed by incorporating ensemble-based techniques, and they remain widely used today. However, standard EnKFs necessitate simplifying assumptions to remain computationally feasible for high-dimensional systems, as the number of samples required to accurately estimate the distribution scales linearly with the system’s dimensionality. On the other hand, more sophisticated methods, such as variational approaches (3D/4D-Var) [36], offer improved assimilation power but demand multiple propagations of the system during optimization, resulting in high computational costs.

To address these limitations, [3] introduced the Ensemble Score Filter (EnSF), which has demonstrated strong performance in high-dimensional, nonlinear data assimilation problems. Unlike EnKF, which uses a set of Monte Carlo samples to represent the probability distribution, EnSF encodes probability density information into a score function and generates samples by solving reverse-time stochastic differential equations (SDEs) based on these scores. However, EnSF encounters challenges in scenarios with sparse observational data, as the score function becomes ill-posed and vanishes in regions with insufficient observations.

A recent method, Latent-EnSF [43], addresses the challenge of sparse observations by employing Variational Autoencoders (VAEs) [24] to project observations and states into a shared latent space. The system dynamics are then evolved in the original full space using the existing simulation method. While this approach is compatible with any numerical or data-driven model, it remains complex and computationally demanding for large-scale applications such as weather forecasting. By the integration of data-driven surrogate models like FourCastNet [32], Graphcast [27], or Pangu Weather [5], the computational challenges can be alleviated, as shown in [46, 43], but may still remain due to the intricate architectures required to model full-space dynamics effectively.

To address the computational challenges associated with simulating full-space dynamics, several methods have been proposed to learn system dynamics directly in latent space [39, 31, 45, 18]. However, many of these approaches rely on model reduction and surrogate models that operate independently, often resulting in oscillatory latent states that are challenging to model. To overcome these limitations, Latent Dynamics Networks (LDNets) [37] and their extension [40] have been developed to jointly identify a low-dimensional latent space and learn the spatiotemporal dynamics within it. This unified approach eliminates the need for operations in the high-dimensional full space, demonstrating improved accuracy while requiring significantly fewer trainable parameters.

However, LDNets require predefined model parameters to initialize and evolve the system’s state, and uncertainty in these parameters can lead to significant deviations over time. To address this issue, we propose a hybrid approach that combines the strengths of LDNets and Latent-EnSF, introducing the **Latent Dynamics Ensemble Score Filter (LD-EnSF)** (Fig.1). This approach integrates the advantages of both methods to mitigate their respective limitations. Furthermore, we incorporate a Long Short-Term Memory (LSTM) [21] encoder for mapping observations to the latent space, enabling the efficient use of past observations, especially in scenarios with high observation sparsity. Our numerical experiments demonstrate that the LD-EnSF method achieves robustness, high accuracy, and significant acceleration compared to EnSF and Latent-EnSF in high-dimensional data assimilation problems with highly sparse and noisy observations.

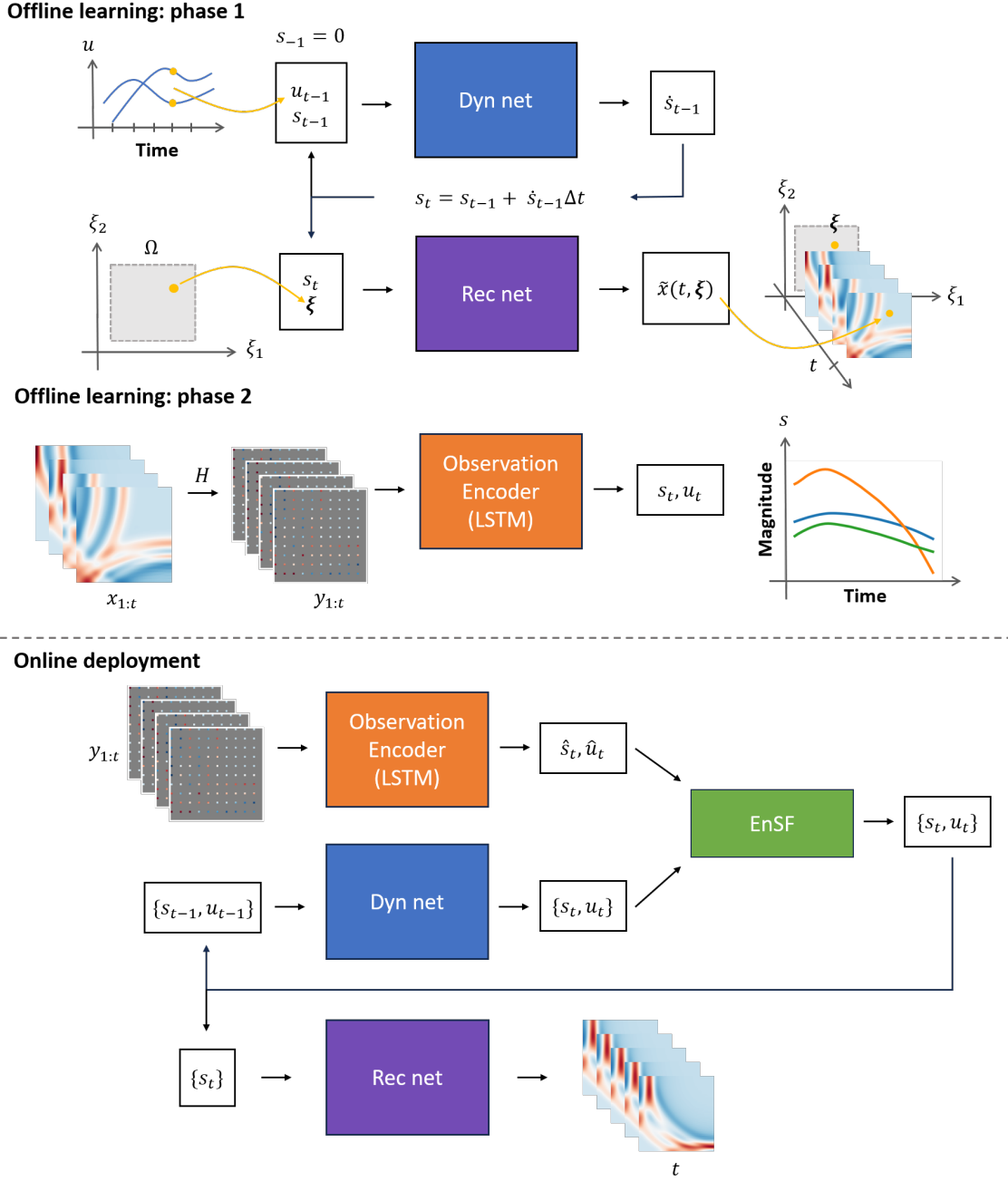


Figure 1: **The pipeline of the LD-EnSF method.** **Offline learning:** In phase 1, the LDNet is trained based on the dataset to capture the latent dynamics. In phase 2, an LSTM encoder is trained to align the observation history $y_{1:t}$ with latent variables s_t and parameters u_t . **Online deployment:** for each assimilation time step, the LD-EnSF assimilates an ensemble of prior latent pairs $\{s_t, u_t\}$ with LSTM encoded latent pairs (\hat{s}_t, \hat{u}_t) . The posterior latent states can then be used to reconstruct the assimilated full states at arbitrary space and temporal points.

1.2 A summary of other related works

Score-based Data Assimilation Methods: Score-based methods have emerged as promising tools for tackling nonlinear data assimilation challenges. [4] introduced the a score-based filter, which integrates score-based diffusion models into a recursive Bayesian filtering framework for state estimation. Additionally, [3] proposed a train-free ensemble score estimation technique, successfully applied to surface quasi-geostrophic dynamics [2], showcasing its effectiveness in complex geophysical systems. In parallel, [38] employed conditional score-based generative models to sample trajectories conditioned on observations, effectively solving smoothing problems by reconstructing entire trajectories using both past and future data. However, these smoothing methods differ from the real-time filtering required in practical applications, where only past and present observations are available for state estimation. More recently, [29] introduced a state-observation augmented diffusion (SOAD) model, which leverages diffusion models to more effectively handle nonlinearities, which is followed by [15] using sequential Langevin sampling with an annealing strategy to enhance convergence and facilitate multi-modal sampling, different from the training-free EnSF we leverage.

Machine Learning for Dynamical Systems: Machine learning has been widely employed to model spatiotemporal dynamics for dimensionality reduction and prediction [39, 10, 31, 45, 18]. These approaches typically begin by compressing the system’s data using dimensionality reduction techniques such as proper orthogonal decomposition (POD) or autoencoders, based on the assumption that the dynamics lie on a low-dimensional manifold. The latent variables’ dynamics are then modeled using architectures like LSTM [21], Neural ODE [12], ReZero [1], DeepONet [30], SINDy [8], or LANO [20]. In contrast, LDNets [37] bypass the need for an autoencoder to compress the high-dimensional space, resulting in a more lightweight and generalizable network architecture.

Latent Dynamics Assimilation: Recent research has explored various approaches for performing data assimilation within latent spaces, leveraging machine learning to improve both accuracy and efficiency [35, 1, 34, 33, 14]. For example, [13] employs Feedforward Neural Networks (FNNs) to evolve latent dynamics, uses a decoder for reconstruction, and integrates the EnKF into the training process to construct surrogate latent dynamics. Similarly, [28] introduces Spherical Implicit Neural Representations to learn the latent space and utilizes NeuralODEs to model the latent dynamics, offering a general framework for latent data assimilation compatible with various Kalman filter algorithms. While these methods primarily focus on Kalman filter-based approaches, our work addresses the challenges of sparse observations in EnSF by incorporating an observation encoder, while maintaining computational efficiency through latent-space assimilation.

The remainder of this paper is organized as follows: Section 2 provides an overview of data assimilation and EnSF and Latent-EnSF methods. Section 3 describes the methodology of LD-EnSF, including a new variant of the architecture of LDNets and a new LSTM encoder for encoding sparse observations. Experimental setups for two dynamical systems including shallow water and Kolmogorov flow, and the performance evaluations and comparisons are detailed in Section 4. Finally, Section 5 concludes with a summary of contributions and directions for future research.

2 Background

In this section, we introduce the foundational concepts and problem setup for data assimilation, present two methods: ensemble sore filter (EnSF) and its latent space variant, Latent-EnSF.

2.1 Problem setup

We denote $x_t \in \mathbb{R}^{d_x}$ as a d_x -dimensional state variable of a dynamical system at (discrete) time $t \in \mathbb{Z}^+$, with initial state x_0 . Given the state x_{t-1} at time $t-1$, with $t = 1, 2, \dots$, the evolution of the state from $t-1$ to t is modeled as

$$x_t = M(x_{t-1}, u_{t-1}), \quad (1)$$

where $u_{t-1} \in \mathbb{R}^{d_u}$ represents a d_u -dimensional uncertain parameter, $M : \mathbb{R}^{d_x} \times \mathbb{R}^{d_u} \rightarrow \mathbb{R}^{d_x}$ is a non-linear forward map. By $y_t \in \mathbb{R}^{d_y}$ we denote a d_y -dimensional noisy observation data, given as

$$y_t = H(x_t) + \gamma_t. \quad (2)$$

where $H : \mathbb{R}^{d_x} \rightarrow \mathbb{R}^{d_y}$ is the observation map, and γ_t represents the observation noise.

Due to the model inadequacy and input uncertainty, the model of the dynamical system (1) could lead to inaccurate prediction of the ground truth. The goal of data assimilation is to find the best estimate, denoted by \hat{x}_t , of the ground truth, given the observation data $y_{1:t} = (y_1, y_2, \dots, y_t)$ up to time t . This requires us to compute the conditional probability density function (PDF) of the state, denoted as $P(x_t|y_{1:t})$, which is often non-Gaussian.

In Bayesian filter framework [16], the data assimilation problem becomes evolving $P(x_{t-1}|y_{1:t-1})$ to $P(x_t|y_{1:t})$ from time $t-1$ to t . This includes two steps, a prediction step followed by an update step. In the prediction step, we predict the density of x_t , denoted as $P(x_t|y_{1:t-1})$, from $P(x_{t-1}|y_{1:t-1})$ and the forward evolution of the dynamical model (1) as

$$\textbf{Prediction: } P(x_t|y_{1:t-1}) = \int P(x_t|x_{t-1})P(x_{t-1}|y_{1:t-1})dx_{t-1}, \quad (3)$$

where $P(x_t|x_{t-1})$ represents a transition probability. Then in the update step, given the new observation data y_t , the prior density $P(x_t|y_{1:t-1})$ from the prediction is updated to the posterior density $P(x_t|y_{1:t})$ by Bayes' rule as

$$\textbf{Update: } P(x_t|y_{1:t}) = \frac{1}{Z}P(y_t|x_t)P(x_t|y_{1:t-1}). \quad (4)$$

Here, $P(y_t|x_t)$ is the likelihood function of the observation data y_t determined by the observation model (2), i.e., $P(y_t|x_t) = P_{\gamma_t}(y_t - H(x_t))$ with probability density P_{γ_t} of the observation noise γ_t . Z is the model evidence or the normalization constant given as $Z = \int P(y_t|x_t)P(x_t|y_{1:t-1})dx_t$, which is often intractable to compute.

2.2 Ensemble score filter (EnSF)

To avoid calculating the normalization constant in Eq. (4), the EnSF method [4] proposes to draw samples from the posterior $P(x_t|y_{1:t})$ using its score, i.e., the gradient of Eq. (4)

$$\nabla_x \log P(x_t|y_{1:t}) = \nabla_x \log P(x_t|y_{1:t-1}) + \nabla_x \log P(y_t|x_t), \quad (5)$$

taken with respect to x_t , which eliminates Z .

The EnSF exploits the score function to sample from the posterior distribution using recent advances in score-based stochastic differential equations (SDEs) [44]. At given physical time t , we define a pseudo diffusion time $\tau \in \mathcal{T} = [0, 1]$, at which we progress

$$\textbf{Forward SDE: } dx_{t,\tau} = f(x_{t,\tau}, \tau)d\tau + g(\tau)dW, \quad (6)$$

driven by a d_x -dimensional Wiener process W . Here we use $x_{t,\tau}$ to indicate the state at physical time t and diffusion time τ . The drift term $f(x_{t,\tau}, \tau)$ and the diffusion term $g(\tau)$ are chosen as

$$f(x_{t,\tau}, \tau) = \frac{d \log \alpha_\tau}{d\tau} x_{t,\tau}, \quad g^2(\tau) = \frac{d\beta_\tau^2}{d\tau} - 2 \frac{d \log \alpha_\tau}{d\tau} \beta_\tau^2, \quad (7)$$

with $\alpha_\tau = 1 - \tau(1 - \epsilon_\alpha)$ and $\beta_\tau^2 = \tau$, where ϵ_α is a small positive hyperparameter to avoid $d \log \alpha_\tau / d\tau$ being not defined at $\tau = 1$. This choice leads to the conditional Gaussian distribution

$$x_{t,\tau} | x_{t,0} \sim \mathcal{N}(\alpha_\tau x_{t,0}, \beta_\tau^2 I), \quad (8)$$

which gradually transforms the data distribution taken as $x_{t,0} = x_t \sim P(x_t | y_{1:t})$ at $\tau = 0$ close to a standard normal distribution at $\tau = 1$. This transformation process can be reversed by progressing

$$\textbf{Reverse-time SDE: } dx_{t,\tau} = [f(x_{t,\tau}, \tau) - g^2(\tau) \nabla_x \log P(x_{t,\tau} | y_{1:t})] d\tau + g(\tau) d\bar{W}, \quad (9)$$

where \bar{W} is another Wiener process independent of W , and $\nabla_x \log P(x_{t,\tau} | y_{1:t})$ is the score of the density $P(x_{t,\tau} | y_{1:t})$ with the gradient ∇_x taken with respect to $x_{t,\tau}$. By this formulation, $x_{t,\tau}$ follows the same distribution with density $P(x_{t,\tau} | y_{1:t})$ in the forward and reverse-time SDEs.

To compute the score $\nabla_x \log P(x_{t,\tau} | y_{1:t})$ in Eq. (9), EnSF [4] uses

$$\nabla_x \log P(x_{t,\tau} | y_{1:t}) = \nabla_x \log P(x_{t,\tau} | y_{1:t-1}) + h(\tau) \nabla_x \log P(y_t | x_{t,\tau}), \quad (10)$$

where the damping function $h(\tau) = 1 - \tau$ is chosen to monotonically decrease in $[0, 1]$, with $h(1) = 0$ and $h(0) = 1$. The likelihood function $P(y_t | x_{t,\tau})$ in the second term can be explicitly derived from the observation map Eq. (2). For the first term, by $P(x_{t,\tau} | y_{1:t-1}) = \int P(x_{t,\tau} | x_{t,0}) P(x_{t,0} | y_{1:t-1}) dx_{t,0}$ and the conditional Gaussian distribution Eq. (8), we have the prior score

$$\nabla_x \log P(x_{t,\tau} | y_{1:t-1}) = \int -\frac{x_{t,\tau} - \alpha_\tau x_{t,0}}{\beta_\tau^2} \omega(x_{t,\tau}, x_{t,0}) P(x_{t,0} | y_{1:t-1}) dx_{t,0}, \quad (11)$$

where the weight is given by

$$\omega(x_{t,\tau}, x_{t,0}) = \frac{P(x_{t,\tau} | x_{t,0})}{\int P(x_{t,\tau} | x'_{t,0}) P(x'_{t,0} | y_{1:t-1}) dx'_{t,0}}. \quad (12)$$

Both the prior score function in Eq. (11) and the weight in Eq. (12) can be approximated using Monte Carlo approximation, with samples drawn from distribution $P(x_{t,0} | y_{1:t-1})$ in Eq. (3).

With the score function $\nabla_x \log P(x_{t,\tau} | y_{1:t})$ evaluated as in Eq. (10), the samples from the target distribution $P(x_t | y_{1:t})$ can be generated by first drawing samples from $\mathcal{N}(0, I)$ and then solving the reverse-time SDE Eq. (9) using, e.g., Euler-Maruyama scheme. To summarize, the workflow of one step data assimilation by EnSF is presented in Algorithm. 1.

Algorithm 1 One step of EnSF

Input: Ensemble of the states $\{x_{t-1}\}$ from distribution $P(x_{t-1} | y_{1:t-1})$ and new observation y_t .

Output: Ensemble of the states $\{x_t\}$ from distribution $P(x_t | y_{1:t})$.

Simulate the forward model (1) from $\{x_{t-1}\}$ to obtain samples $\{x_{t,0}\}$ following $P(x_t | y_{1:t-1})$.

Generate random samples $\{x_{t,1}\}$ from standard normal distribution $N(0, I)$.

Solve the reverse-time SDE (9) starting from samples $\{x_{t,1}\}$ using the score (10) to obtain $\{x_t\}$.

EnSF leverages the explicit likelihood function and the diffusion process to generate samples without assuming approximate linearity of the dynamical system. It has been demonstrated accurate and scalable for data assimilation of nonlinear and high-dimensional systems, such as the Lorenz 96 system with one million dimensions [3] and the inherently chaotic quasi-geostrophic surface model [2]. However, a key limitation of EnSF is that the score of the likelihood function may vanish at unobserved components or dimensions of the state [43], which significantly limits the performance of EnSF when the observation data is sparse, or only a small number of components or dimensions of the state are observed.

2.3 Latent-EnSF

To address the limitation of EnSF for data assimilation with sparse observations, [43] developed Latent-EnSF to conduct data assimilation in a latent space. It avoids the vanishing score by learning a shared latent space into which both the states x_t and the observations y_t are encoded. They train a coupled variational autoencoder (VAE) with state encoder $\mathcal{E}_{\text{state}}$, observation encoder \mathcal{E}_{obs} , and decoder \mathcal{D} , where they minimize a loss function with three terms, one term accounting for the discrepancy between the latent representations of the state and observation, one term measuring the errors of the reconstruction of the full states from the latent representations, and one term on regularization of the latent distributions by a standard normal distribution.

Once trained, the coupled VAE enables data assimilation by running the EnSF algorithm in the latent space with encoded representations $\mathcal{E}_{\text{state}}(\{x_t\})$ of the ensemble states $\{x_t\}$ and the encoded observation given by $\mathcal{E}_{\text{obs}}(y_t)$. The assimilated latent state samples are then decoded back into the full state space, which are taken as the samples of the posterior distribution with density $P(x_t|y_{1:t})$. These samples at time t are then propagated to the next time $t + 1$ by simulating the dynamical model (1). The Latent-EnSF effectively overcame the challenge of vanishing scores in scenarios with sparse observations, achieving high assimilation accuracy. For example, it maintained the same accuracy as the EnSF with full observations while using only 0.44% of the state components as observations for a shallow water wave propagation problem. In contrast, under such extreme sparsity, the EnSF exhibited substantial assimilation errors, nearly equivalent to the errors of the dynamics from the ground truth in the absence of any data assimilation.

Beyond the improved accuracy, Latent-EnSF was also demonstrated more efficient than EnSF in drawing samples by the score-based diffusion process in the latent space. However, data assimilation using Latent-EnSF still involves the simulation of the forward dynamical model (1) at each of the assimilation step, which could be expensive and become prohibitive for using a large number of samples and for conducting data assimilation fast enough in real-time applications. We propose to break this limitation and empower Latent-EnSF by leveraging latent dynamics to achieve fast data assimilation without simulating the full dynamical model (1).

3 Methodology

To avoid simulating the full dynamical model (1) for fast data assimilation, we propose to construct and integrate latent dynamics, a dynamical model for a latent representation of the full state, in the data assimilation process. Specifically, we propose to integrate a latent dynamical model using a variant of Latent Dynamics Networks (LDNets) developed in [37]. To align the observation data with the latent states, we leverage their temporal correlation and propose encoding the data into the same latent space using an LSTM. This encoded latent data are then assimilated into the latent states using EnSF, operating in a significantly lower-dimensional latent space compared

to the original state space. This approach enables rapid data assimilation without requiring full dynamics simulation.

3.1 Latent dynamics networks (LDNets)

LDNet is a novel neural network architecture that is able to discover and maintain low-dimensional dynamical latent representation of the full dynamics [37]. The LDNet consists of a dynamics network and a reconstruction network. The dynamics network evolves the dynamics of latent variables, while the reconstruction network converts latent states back to full states, conditioned on spatial points. It is able to predict the time evolution of space-dependent fields at any given spatial point in a mesh free manner. Consider a function space \mathcal{X} of functions x defined on a temporal-spatial physical domain $\mathcal{T} \times \Omega \subset \mathbb{R} \times \mathbb{R}^{d_\xi}$:

$$x : \mathcal{T} \times \Omega \ni (t, \xi) \mapsto x(t, \xi),$$

where $\mathcal{T} = [0, T] \in \mathbb{R}$ is the time domain and $\Omega \subset \mathbb{R}^d$ is the space domain. Consider that the evolution of the state x in time depends on the parameter $u \in \mathcal{U}$ of the dynamical system

$$u : \mathcal{T} \ni t \mapsto u(t).$$

To accommodate varying initial condition of the state $x(0) = x_0$, we propose a variant of the LDNets from [37], which consists of two sub-networks, i.e., a dynamics network \mathcal{F}_{θ_1} and a reconstruction network \mathcal{R}_{θ_2} , where θ_1 and θ_2 denote the corresponding trainable parameters. The dynamics network \mathcal{F}_{θ_1} , see Fig. 1, takes as input the latent state $s_{t-1} \in \mathbb{R}^{d_s}$ and the parameter $u_{t-1} = u(t-1)$ at time $t-1$ and output the time derivative of s_{t-1} , i.e.,

$$\dot{s}_{t-1} = \mathcal{F}_{\theta_1}(s_{t-1}, u_{t-1}), \quad t = 0, 1, 2, \dots, \quad (13)$$

The latent state s_t evolves according to the output of dynamics network

$$s_t = s_{t-1} + \Delta t \dot{s}_{t-1}, \quad t = 0, 1, 2, \dots, \quad (14)$$

with a time step Δt , e.g., uniformly taken as $\Delta t = T/n$ for n steps. We set the initial condition at $t = -1$ as $s_{-1} = 0$ (compared to [37] with $s_0 = 0$). The reconstruction network, see Fig. 1, outputs an approximate full state $\tilde{x}(t, \xi)$ from the latent state s_t at any query point $\xi \in \Omega$ as

$$\tilde{x}(t, \xi) = \mathcal{R}_{\theta_2}(s_t, \xi), \quad t = 0, 1, 2, \dots$$

For the training of the LDNet, the loss function is chosen as

$$\mathcal{L}(\theta_1, \theta_2) = \frac{1}{NMn} \sum_{j=1}^N \sum_t \sum_{\xi} |\tilde{x}_j(t, \xi) - x_j(t, \xi)|^2, \quad (15)$$

where $\{x_j\}_{j=1}^N$ denote N trajectories sampled from \mathcal{X} corresponding to N samples of the parameter u , and M is the number of spatial points ξ in each trajectory. We propose a two-stage training of the LDNet. In the first stage, we train both the dynamics network and the reconstruction network until convergence. In the second stage, we only retrain the reconstruction network with fixed latent representations, which is demonstrated to achieve lower reconstruction errors.

3.2 Encoding observations to match latent representations

We draw inspiration from the Latent-EnSF [43], which conducts data assimilation by applying the EnSF in the latent space. While the Latent-EnSF enables high-dimensional data assimilation, it still requires computing the dynamics in the original space, which can be computationally expensive, especially for complex dynamics. By leveraging LDNets, both the assimilation and evolution of dynamics can be performed in the low-dimensional latent space, significantly reducing the computational cost. Additionally, unlike the VAEs used in Latent-EnSF with two coupled encoders in encoding the states and observations, LDNets compute the latent states for every input parameter by running a latent dynamics. This design allows the use of a single encoder to encode the observations, which is trained to align the observations with the latent states.

The VAE observation encoder in Latent-EnSF maps observations at time t to a latent variable that is trained to align with the latent state encoded from the full state by the state encoder. This observation map may be insufficient to construct an accurate latent representation, especially if the observations are very sparse and noisy at a single time step t . To address this issue, we propose to use Long Short-Term Memory (LSTM) networks [21] as the observation encoder. LSTMs are specifically designed to capture long-term dependencies in sequential data, such as time-dependent observations y_t , latent states s_t , and parameters u_t . Each LSTM unit contains memory cells that retain information over time, along with input, output, and forget gates that regulate the flow of information, enabling the network to learn both short-term and long-term memories. To align with the dynamics propagation within the LDNet framework, we propose to match the observations $y_{1:t}$ up to time t with both the latent state s_t and the parameter u_t at time t , as illustrated in Fig. 1 on the offline learning phase 2.

The LSTM encoder network, denoted as $\mathcal{E}_{\theta_3} : \mathbb{R}^{d_y+d_h} \rightarrow \mathbb{R}^{d_u+d_s}$, is parameterized by trainable parameters θ_3 and incorporates a hidden observation $h_t \in \mathbb{R}^{d_h}$ at each time step t . The output of the LSTM network is a pair of the approximate latent state $\hat{s}_t \in \mathbb{R}^{d_s}$ and parameter $\hat{u}_t \in \mathbb{R}^{d_u}$:

$$(\hat{s}_t, \hat{u}_t) = \mathcal{E}_{\theta_3}(y_t, h_t), \quad (16)$$

where $y_t = H(x_t)$ is the noiseless sparse observation data at time t , and the hidden observation h_t includes all historical noiseless observation data $y_{1:t-1}$. To train the LSTM encoder, we minimize the following loss function

$$\mathcal{L}(\theta_3) = \frac{1}{Nn} \sum_{j=1}^N \sum_t \left(\left| \hat{s}_t^{(j)} - s_t^{(j)} \right|^2 + \left| \hat{u}_t^{(j)} - u_t^{(j)} \right|^2 \right), \quad (17)$$

for N trajectories corresponding to the training of the LDNet. Note that by matching both the latent state s_t and the parameter u_t with the output of the LSTM network, we can also estimate the parameter in the data assimilation process, which is not considered in Latent-EnSF.

3.3 Latent dynamics ensemble score filter (LD-EnSF)

Once the LDNet and the LSTM are constructed, we can perform data assimilation in the latent space by EnSF with the latent dynamics and the latent observations, as shown in Fig. 1. Let $\kappa_t = (s_t, u_t)$ denote the augmented latent state, with the latent state s_t of the dynamics network evolving as in (14). Let $\phi_t = (\hat{s}_t, \hat{u}_t)$ denote the corresponding latent observation data encoded by the LSTM network. The the latent observation data can be approximately modeled as

$$\phi_t = H_{\text{latent}}(\kappa_t) + \hat{\gamma}_t, \quad (18)$$

where we take $H_{\text{latent}}(\kappa_t) = \kappa_t$, the identity map, with the latent observation noise $\hat{\gamma}_t$ estimated by LSTM encoding of the true observation noise γ_t in (2). To this end, the data assimilation problem in the latent space can be formulated as the prediction step

$$\textbf{Prediction: } P(\kappa_t|\phi_{1:t-1}) = \int P(\kappa_t|\kappa_{t-1})P(\kappa_{t-1}|\phi_{1:t-1})d\kappa_{t-1}, \quad (19)$$

with the transition probability $P(\kappa_t|\kappa_{t-1})$ derived from the latent dynamics, and the update step

$$\textbf{Update: } P(\kappa_t|\phi_{1:t}) = \frac{1}{Z}P(\phi_t|\kappa_t)P(\kappa_t|\phi_{1:t-1}), \quad (20)$$

with likelihood function $P(\phi_t|\kappa_t)$ and normalization constant Z . Then, we can employ EnSF from Section 2.2 to solve this data assimilation problem, with both the dynamics and the observations performed in the latent space. We present one step of the LD-EnSF in Algorithm 2.

Algorithm 2 One step of LD-EnSF

Input: Ensemble of the latent states and parameters $\{\kappa_{t-1}\}$ from distribution $P(\kappa_{t-1}|\phi_{1:t-1})$ and the observation y_t . Dynamics network \mathcal{F}_{θ_1} , observation encoder \mathcal{E}_{θ_3} , and hidden observation h_t .

Output: Ensemble of the latent states and parameters $\{\kappa_t\}$ from distribution $P(\kappa_t|\phi_{1:t})$.

Encode the new observation y_t and hidden observation h_t into latent space $\phi_t = \mathcal{E}_{\theta_3}(y_t, h_t)$

Simulate the latent dynamics (14) from $\{\kappa_{t-1}\}$ to obtain samples $\{\kappa_{t,0}\}$ following $P(\kappa_t|\phi_{1:t-1})$.

Generate random samples $\{\kappa_{t,1}\}$ from standard normal distribution $N(0, I)$.

Solve the reverse-time SDE (9) starting from samples $\{\kappa_{t,1}\}$ using the score (10) to obtain $\{\kappa_t\}$.

The LD-EnSF process is illustrated in Fig. 1 online deployment part. The assimilation loop operates entirely within the latent space, eliminating the need to transform back to the full space. Once the assimilation is complete, providing the required latent states, the reconstruction network enables evaluation of the full state at any spatial point and time step. Additionally, the smoothness of the latent states, as demonstrated in our numerical experiments in Section 4.2, allows for interpolation between time steps, so the full state can be evaluated at any continuous time point.

4 Experiments

4.1 Test cases

To demonstrate the accuracy of the LDNet approximation and LD-EnSF assimilation and their computational efficiency, we test on two complex examples, including water wave propagation based on simplified shallow water equations with random initial conditions and Kolmogorov flow based on Navier–Stokes equations with random Reynolds number.

Shallow water equations: We consider shallow water equations, which are widely used to model the propagation of shallow water where the vertical depth of the water is much smaller than the horizontal scale. These equations are frequently applied in oceanographic and atmospheric fluid dynamics. In this study, we adopt a simplified form of the shallow water equations:

$$\begin{aligned} \frac{d\mathbf{v}}{dt} &= -g\nabla\eta, \\ \frac{d\eta}{dt} &= -\nabla \cdot ((\eta + H)\mathbf{v}), \end{aligned} \quad (21)$$

where \mathbf{v} is the two-dimensional velocity field, and η represents the surface elevation. Both \mathbf{v} and η constitute the system states to be assimilated. Here, $H = 100\text{m}$ denotes the mean depth of the fluid, and g is the constant representing gravitational acceleration. We define a two-dimensional domain of size $L \times L$, where $L = 10^6\text{m}$ in each direction. The initial condition is a displacement of the surface elevation modeled by a randomly located local Gaussian bump perturbation from the flat surface. The boundary conditions are set such that $\mathbf{v} = 0$. Over time, the wave dynamics becomes increasingly complex due to reflections at the boundaries. The spatial domain is discretized into a uniform grid of 150×150 , following the setup in [43]. The simulation is carried out over 2000 time steps using an upwind scheme with a time step size of $\delta t \approx 21$ seconds. Including the initial condition, the dataset comprises 2001 time steps. We generate 200 trajectories, dividing them into training (60%), validation (20%), and evaluation (20%) sets.

Kolmogorov flow: In the second example, we consider the Kolmogorov flow with an uncertain Reynolds number, a parametric family of statistically stationary turbulent flows driven by body force. This incompressible fluid is governed by the Navier-Stokes equation [25]:

$$\begin{aligned} \frac{d\mathbf{v}}{dt} &= -\mathbf{v} \cdot \nabla \mathbf{v} + \frac{1}{Re} \nabla^2 \mathbf{v} - \frac{1}{\rho} \nabla p + \mathbf{f}, \\ \nabla \cdot \mathbf{v} &= 0, \end{aligned} \tag{22}$$

where the external forcing term \mathbf{f} is defined as $\mathbf{f} = \sin(4\xi_2)\hat{\xi}_1 - 0.1\mathbf{v}$, where $\boldsymbol{\xi} = (\xi_1, \xi_2)$ is the spatial coordinate, $\hat{\xi}_1 = (1, 0)$, \mathbf{v} is the velocity field, p is the pressure field, and $\rho = 1$ denotes the fluid density. The fluid velocity \mathbf{v} is the state variable to be assimilated. The spatial domain is defined as $[0, 2\pi]^2$ with periodic boundary conditions and a fixed initial condition. The flow complexity is controlled by the Reynolds number Re . The spatial resolution is set as 150×150 . We simulate the flow over 300 time steps with a step size of $\delta t = 0.04$ and take the data from time steps 100 to 300. A total of 200 trajectories are generated, with the Reynolds number (Re) randomly sampled from the range $[500, 1500]$. These trajectories are divided into training (60%), validation (20%), and evaluation (20%) sets.

Prior to training, we normalize the data following the approach of [37]. For bounded data, we scale variables, including the parameter u , the space coordinate ξ , and the state variable x , to the range $[-1, 1]$. For unbounded data, we standardize the variables so that they have a mean of 0 and a variance of 1. The time step Δt in (14) is treated as a tunable hyperparameter during training.

4.2 Offline learning of the LDNets

We learn LDNets as latent dynamical surrogate models of the full dynamical models for the two test examples from the normalized training dataset. We employ hyperparameter search [6] for the training of the LDNets, including the architecture of the dynamics network, the reconstruction network, the dimension of the latent states, the optimization parameters, see details in Table 2.

For the shallow water equations, the spatial coordinates of the initial Gaussian bump serve as the input parameter (u). For the training of the LDNet (13) with the loss function (15), by a hyperparameter search (see details in Table 2), we take one state in every 40 time steps, resulting in $n = 51$ latent states, s_0, s_1, \dots, s_{50} , in one trajectory. We take $M = 5000$ spatial points randomly selected from 150×150 grid points or each time step and trajectory. Notice that these numbers of downsampled time steps and spatial points can also be set as hyperparameters and tuned during the training process. The hyperparameter search (Table 2) determines the latent state dimension as 10, the dynamic network as a fully-connected neural network with a depth of 8 and a width

of 50, and the reconstruction network as fully-connected neural network with a depth of 7 and a width of 180. The training details are listed in Table 3. The training results, illustrated in top-left panel of Fig. 2, indicate that LDNets achieve an average test error of 1.6%, outperforming the 6.8% test error observed for the VAE in Latent-EnSF [43]. Here the test errors are measured in relative root mean square error (RMSE). To further enhance performance, we fix the dynamics network and retrain the reconstruction network to better align the latent states with full states. This additional step reduces the average test error from 1.6% to 1.2%, see a comparison of the ground truth full dynamics (first row) and the LDNets predictions (second row) as well as the errors (third row) for a test sample in Fig. 3.

For the Kolmogorov flow example, the Reynolds number Re serves as the input parameter (u). The training dataset is downsampled from 200 time steps to 40 time steps by taking the states every 5 time steps, with 5000 random spatial points selected per time step. Through hyperparameter search (see details in Table 2), the latent state dimension is determined to be 9, while the dynamics network is configured with a depth of 9 and width of 200, and the reconstruction network has a depth of 15 and a width of 500. As shown in the bottom-left panel of Fig. 2, the VAE in Latent-EnSF exhibits a test error of 6.4%. In comparison, LDNets achieve a test error of 3.4%, which further reduce to 2.0% after retraining the reconstruction network.

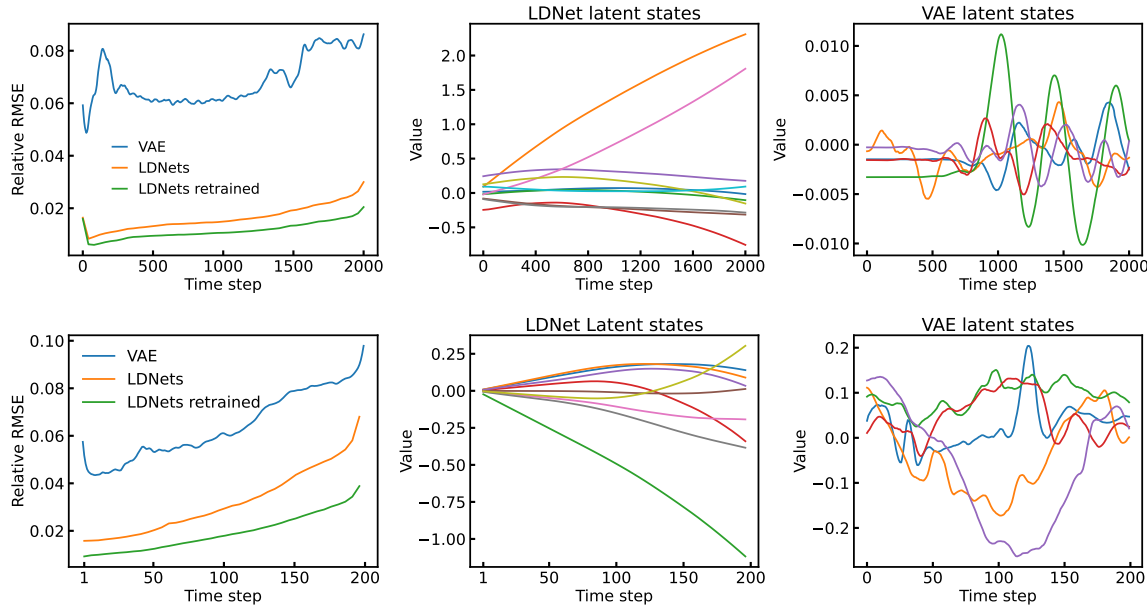


Figure 2: Comparison of the reconstruction errors (left) of the VAE and LDNets (with and without retraining of the reconstruction network) for the shallow water equations (top) and Kolmogorov flow (bottom). The latent states of LDNets (middle) are much smoother than those of VAE (right).

Smoothness of the latent state: The middle and right panels of Fig. 2 compare the trajectories of the latent states from LDNets with part of those of the mean latent states from VAEs. The latent state produced by LDNets is noticeably smoother. This smoothness makes the assimilation of observation data with the latent state easier and helps to achieve higher assimilation accuracy. Moreover, it enables interpolation of the latent states over time and allows the full states to be reconstructed at any continuous time point with interpolated latent states. In contrast, the latent space of VAEs tends to be more oscillatory, posing challenges in constructing a stable latent

surrogate model as attempted in our experiments.

4.3 Offline learning of the observation encoder

After training LDNets, we obtain a sequence of the latent states s_t in (14) for every input parameter sequence u_t by running the latent dynamical model (13). We map the sequence of observations using the LSTM encoder (16) to the latent states and parameters by minimizing the loss function (17) over all training trajectories, as shown in Fig. 1.

The observation operator H is set as a sparse sub-sampling matrix that selects the state values uniformly from 10×10 out of 150×150 grid points, as shown in the fourth row of Fig. 3 and Fig. 4. This corresponds to only 0.44% of the total number of grid points. The training data of the observations at this stage do not include observation noise. For the first example of the shallow water wave propagation, we use an LSTM network with a width of 256 and two hidden layers. After training, the LSTM encoder achieves an average test error of 1.50% on the latent states and parameters in the test dataset. For Kolmogorov flow example, employing an LSTM network with a single hidden layer of width 128 results in an average test error of 0.20%. Detailed training configurations are provided in Table 4.

4.4 Online deployment of LD-EnSF

We integrate LDNet as a surrogate for the full dynamics and utilize the LSTM encoded observations to perform data assimilation in the latent space using EnSF. The assimilated latent states are then reconstructed into full states via the reconstruction network, as illustrated in Fig. 1 for the online deployment of LD-EnSF. We demonstrate LD-EnSF’s capability to handle high-dimensional data assimilation problems with sparse observations through applications to both shallow water wave dynamics and Kolmogorov flow.

For the shallow water equations, we initialize an ensemble of 20 samples $\{s_{-1}, u_{-1}\}$, each comprising a pair of the latent state s_{-1} and parameter u_{-1} . Here, $s_{-1} = 0$, and each u_{-1} is randomly drawn from a uniform distribution in the physical domain, representing the coordinates of the local Gaussian bump used to model the initial surface elevation. We consider noisy observations that are sparse in both space and time, with spatially sparse observations at 10×10 from 150×150 spatial grid points (see the fourth row in Fig. 3) and temporally sparse observations at every 40 time steps of the ground truth full dynamics of 2000 time steps (see the top row of Fig. 3 at five time steps). We run the LD-EnSF Algorithm 2 to assimilate the LSTM encoded noisy observation data (with 10% noise) to the latent states. The reconstructed full states at one assimilated sample of the latent states are as shown in the fifth row of Fig. 3, with small assimilation errors shown in the last row.

For the Kolmogorov flow example, we also initialize an ensemble of 20 samples $\{s_{-1}, u_{-1}\}$, with $s_{-1} = 0$ and the Reynolds number parameter u_{-1} randomly sampled from the uniform distribution in $[500, 1500]$. For the noisy (with 10% noise) and sparse observations (see the fourth row of Fig. 4), we consider one observation in every 5 time steps of the full dynamics (1st row of Fig. 4) at Reynolds number $Re = 1469.5$, resulting in 40 observation steps out of 200 total time steps. A trajectory of the perturbed dynamics at Reynolds number $Re = 545.2$ and its increasing difference in time from the truth dynamics are shown in the second and third rows of Fig. 4. Running the LD-EnSF Algorithm 2, we obtain the full dynamics (5th row of Fig. 4), which are reconstructed from an assimilated sample of the latent states. Much smaller errors of the assimilated dynamics can be observed (6th row of Fig. 4) compared to the perturbed dynamics.

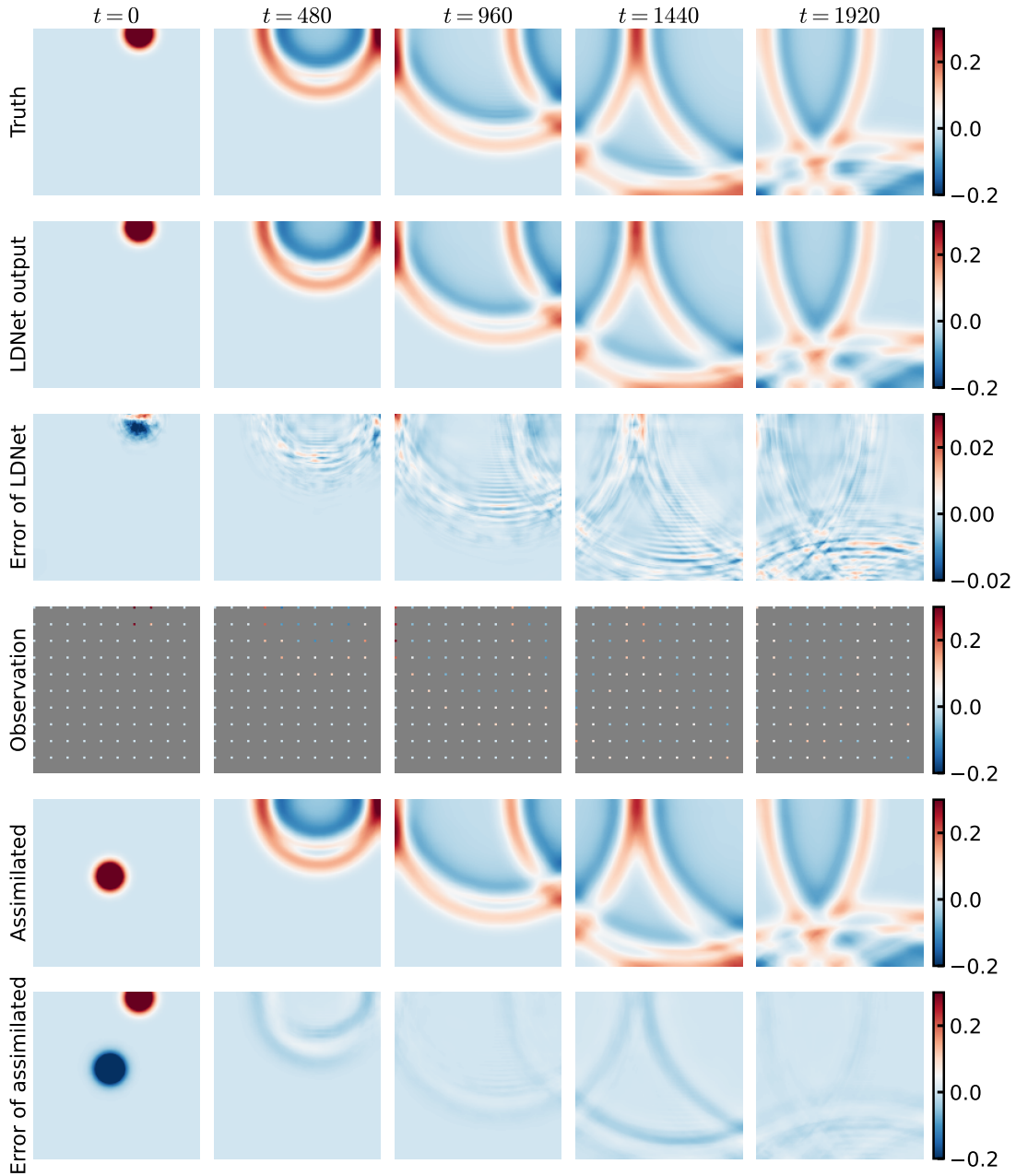


Figure 3: Visualization of the ground truth of the surface elevation η of the shallow water dynamics (21) (1st row), LDNet predictions from known initial condition (2nd row), and the prediction errors (3rd row) at five time steps. Sparse observations at 10×10 from 150×150 spatial grid points (4th row) are assimilated to an ensemble of 20 samples of the LDNet dynamics starting from 20 random initial conditions by the LD-EnSF algorithm, which leads to the full states (5th row) reconstructed from one sample of the assimilated latent states, with assimilation errors (last row).

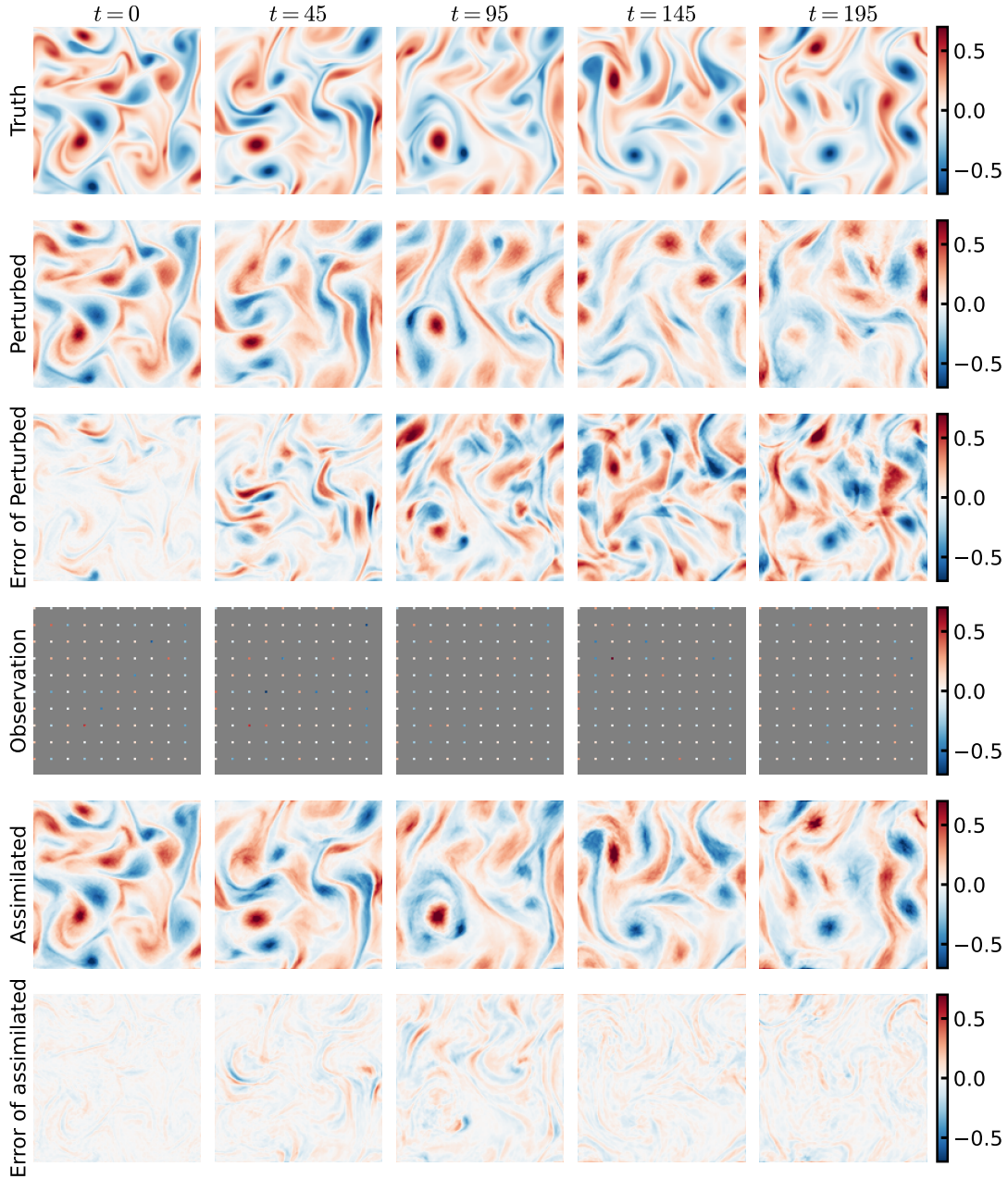


Figure 4: Visualization of the vorticity field $\omega = \nabla \times \mathbf{v}$ of the ground truth of the Kolmogorov flow (22) at Reynolds number $Re = 1469.5$ (1st row) and the perturbed dynamics at $Re = 545.2$ (2nd row), with their difference shown in the 3rd row. Sparse observations (4th row) at 10×10 from 150×150 spatial grid points are assimilated to an ensemble of 20 samples of the LDNet dynamics starting from 20 random samples of the Reynolds number, which leads to the full states (5th row) reconstructed from one sample of the assimilated latent states, with assimilation errors (last row).

4.5 Robustness, accuracy, and efficiency

Both the LDNet and the LSTM encoder are trained on the data without noise. To examine the robustness of the LD-EnSF method with respect to observation noise, we conduct data assimilation experiments with different levels (no noise, 5%, 10%, and 20%) of observation noise for both examples. The relative RMSE of the assimilated latent states and parameters, as well as the reconstructed full states are shown in Fig. 5. Although the assimilation errors for all quantities increase as observation noise grows in both examples, the increase remains modest, and the errors decrease significantly during the initial phase of the assimilation process. This highlights the robustness of LD-EnSF even under large observation noise. We remark that the high assimilation accuracy is achieved not only for the full states, but also for the parameters of the complex dynamical systems with highly sparse (in both space and time) and noisy observations.

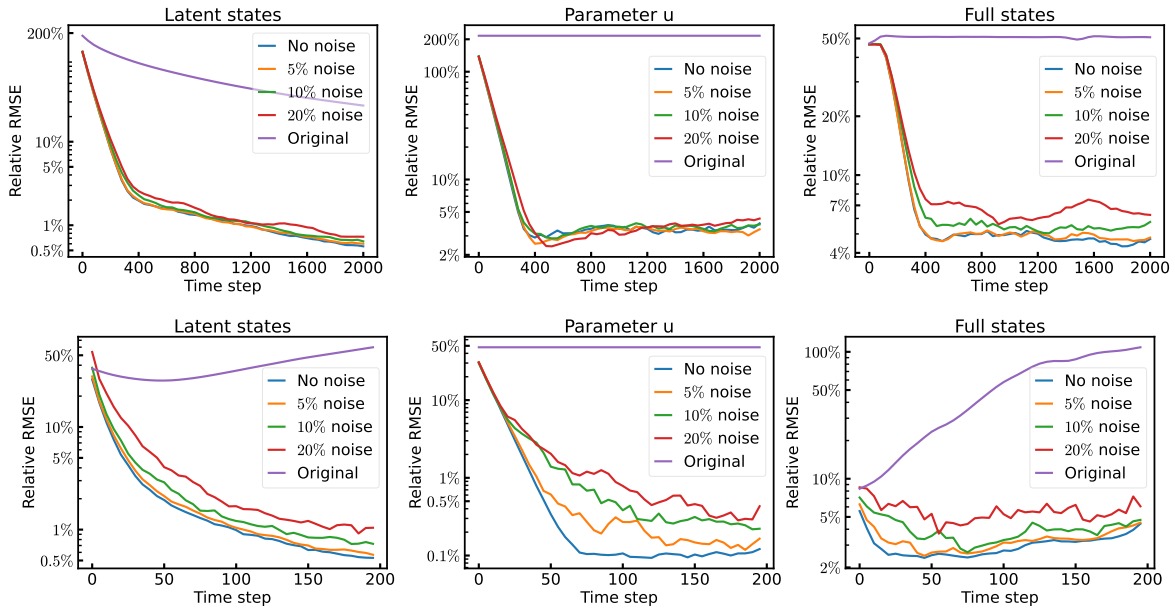


Figure 5: The relative RMSE of the assimilated latent states (left) and parameters (middle) compared to the latent states at the truth parameters, as well as the reconstructed full states (right) at different time steps and observation noises for the shallow water equations (top) and Kolmogorov flow (bottom). The errors of the unassimilated/original quantities are also shown in the plots.

We compare the accuracy of the assimilation by EnSF, Latent-EnSF, and LD-EnSF for the same settings of ensemble sizes, sparse observations, and observation noise. For the training of the Latent-EnSF and LD-EnSF, we also use the same amount of training data. The relative RMSE of the full states, which are assimilated by EnSF and reconstructed by Latent-EnSF and LD-EnSF from the assimilated latent states, are shown in Fig. 6. We can observe that EnSF fails to assimilate sparse observations, with the assimilation errors remaining very large across all time steps. LD-EnSF achieves much higher assimilation accuracy than both EnSF and Latent-EnSF for both examples, especially with the presence of observation noise. This implies that the noisy observations encoded by the LSTM encoder in LD-EnSF are more informative than those encoded by VAE encoder in Latent-EnSF, see the significantly increased assimilation errors when adding noise to the observations by Latent-EnSF on the left panel of Fig. 6. This is likely due to the temporal correlation mechanism exploited by the LSTM encoder. Moreover, we only used a relatively small amount of training data for the LD-EnSF, with one state at partial spatial points

(5,000 out of 22,500) in every 40 time steps for the shallow water equations and every 5 time steps for the Kolmogorov flow in 120 trajectories. High accuracy for both the surrogate approximation and assimilation is achieved. In comparison, the training data of 120 trajectories at all spatial points do not seem to be sufficient for the VAE-based Latent-EnSF to achieve the same accuracy. In fact, many more training data are used in [43].

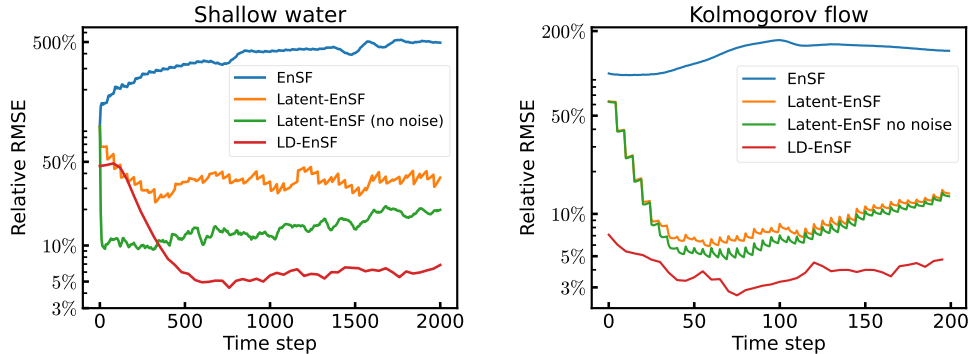


Figure 6: Relative RMSE of the full states assimilated by EnSF and reconstructed from assimilated latent states by Latent-EnSF and LD-EnSF for the shallow water equations (left) and Kolmogorov flow (right). Sparse observations with 10% noise (default) and no noise (for Latent-EnSF) are shown, which indicates the VAE encoding of one step observation with noise is less robust.

We demonstrate the computational efficiency of LD-EnSF in comparison to EnSF and Latent-EnSF. The latter two methods require simulation of the full dynamics in the data assimilation process, while LD-EnSF only evolves a surrogate dynamical model (14) in the prediction step (19). In Table 1, we observe that LD-EnSF achieves 2×10^3 -fold acceleration for the evolution (T_d in Table 1) of the shallow water equations, and 2×10^5 -fold acceleration for the Kolmogorov flow. Besides, as all the steps of the data assimilation are performed in the latent space by LD-EnSF, there is no need to transform the assimilated latent states back to the full space in each step of the data assimilation process. Therefore, comparing to Latent-EnSF for which the latent states are reconstructed/decoded to the full states after each assimilation step, we also save the reconstruction time (T_r in Table 1) if we are only interested in the full states at the final time step. Moreover, LD-Nets learns a very low-dimensional latent representation, ~ 10 dimensions compared to 400 dimensions by Latent-EnSF, which further reduces the assimilation time T_f .

5 Conclusion and future work

In this work, we developed a robust, efficient, and accurate data assimilation method—Latent Dynamics Ensemble Score Filter (LD-EnSF)—for high-dimensional Bayesian data assimilation of large-scale dynamical systems with sparse and noisy observations. We proposed an integration of LD-Nets with a new variant of initialization and retraining and a new LSTM encoding of historical observations. This integration features the combined merits of very low-dimensional and smooth latent representation of the full dynamics, robust and informative encoding of sparse and noisy observations, fast evolution and assimilation of the dynamics in the latent space, joint assimilation of both the states and parameters of the dynamical systems. We demonstrated the robustness, accuracy, and efficiency of LD-EnSF compared to EnSF and Latent-EnSF for two challenging dynamical systems with noisy observations that are highly sparse in both space and time.

Table 1: Comparison of EnSF, Latent-EnSF, and LD-EnSF in terms of running time in seconds. We denote the time for evolution of the dynamics as T_d , the time for data assimilation as T_f , and the time for reconstructing the full state of last time step as T_r . The assimilation dimension is denoted as D_s . All results are for the full trajectory of an ensemble size of 100. The device is AMD 7543 CPU by default, unless GPU (a single NVIDIA RTX A6000 GPU) is specified.

Example	Shallow water			Kolmogorov flow		
Metric	EnSF	Latent-EnSF	LD-EnSF	EnSF	Latent-EnSF	LD-EnSF
T_d (s)	100.95	100.95	0.050	10829.09	10829.09	0.049
T_f (s)	83.86	0.66	0.37	40.13	0.62	0.35
T_r (on GPU) (s)	–	0.78	0.00094	–	0.41	0.0054
D_s	67500	400	12	45000	400	10

Despite the aforementioned advantages of LD-EnSF, there are several avenues for future research. One avenue is to develop more powerful architectures for both the dynamics and reconstruction networks in long-term prediction beyond the training time horizon, especially for more complex dynamical systems with space- and time-dependent uncertain parameters [40]. Another research direction is to theoretically analyze the convergence property of the LD-EnSF in terms of the ensemble size, latent dimensions, observation noise, and sparsity, based on e.g. score approximation and estimation in [11]. Comparison and integration with other data assimilation methods beyond EnSF or score-based methods, e.g., conditional normalizing flow [19], are also interesting.

Acknowledgement

This work is partially supported by NSF grant # 2325631, # 2245111, and # 2245674. We acknowledge helpful discussions with Prof. Felix Herrmann, Yuan Qiu, and Benjamin Burns.

References

- [1] Thomas Bachlechner, Bodhisattwa Prasad Majumder, Henry Mao, Gary Cottrell, and Julian McAuley. Rezero is all you need: Fast convergence at large depth. In *Uncertainty in Artificial Intelligence*, pages 1352–1361. PMLR, 2021.
- [2] Feng Bao, Hristo G Chipilski, Siming Liang, Guannan Zhang, and Jeffrey S Whitaker. Non-linear ensemble filtering with diffusion models: Application to the surface quasi-geostrophic dynamics. *arXiv preprint arXiv:2404.00844*, 2024.
- [3] Feng Bao, Zezhong Zhang, and Guannan Zhang. An ensemble score filter for tracking high-dimensional nonlinear dynamical systems. *arXiv preprint arXiv:2309.00983*, 2023.
- [4] Feng Bao, Zezhong Zhang, and Guannan Zhang. A score-based filter for nonlinear data assimilation. *Journal of Computational Physics*, page 113207, 2024.
- [5] Kaifeng Bi, Lingxi Xie, Hengheng Zhang, Xin Chen, Xiaotao Gu, and Qi Tian. Accurate medium-range global weather forecasting with 3D neural networks. *Nature*, 619(7970):533–538, 2023.

- [6] Lukas Biewald. Experiment tracking with weights and biases, 2020. Software available from wandb.com.
- [7] Craig H Bishop, Brian J Etherton, and Sharanya J Majumdar. Adaptive sampling with the ensemble transform kalman filter. Part I: Theoretical aspects. *Monthly weather review*, 129(3):420–436, 2001.
- [8] Steven L Brunton, Joshua L Proctor, and J Nathan Kutz. Discovering governing equations from data by sparse identification of nonlinear dynamical systems. *Proceedings of the national academy of sciences*, 113(15):3932–3937, 2016.
- [9] Kevin T Carlberg, Antony Jameson, Mykel J Kochenderfer, Jeremy Morton, Liqian Peng, and Freddie D Witherden. Recovering missing CFD data for high-order discretizations using deep neural networks and dynamics learning. *Journal of Computational Physics*, 395:105–124, 2019.
- [10] Kathleen Champion, Bethany Lusch, J Nathan Kutz, and Steven L Brunton. Data-driven discovery of coordinates and governing equations. *Proceedings of the National Academy of Sciences*, 116(45):22445–22451, 2019.
- [11] Minshuo Chen, Kaixuan Huang, Tuo Zhao, and Mengdi Wang. Score approximation, estimation and distribution recovery of diffusion models on low-dimensional data. In *International Conference on Machine Learning*, pages 4672–4712. PMLR, 2023.
- [12] Ricky TQ Chen, Yulia Rubanova, Jesse Bettencourt, and David K Duvenaud. Neural ordinary differential equations. *Advances in neural information processing systems*, 31, 2018.
- [13] Yuming Chen, Daniel Sanz-Alonso, and Rebecca Willett. Reduced-order autodifferentiable ensemble kalman filters. *Inverse Problems*, 39(12):124001, 2023.
- [14] Sibio Cheng, Jianhua Chen, Charitos Anastasiou, Panagiota Angeli, Omar K Matar, Yi-Ke Guo, Christopher C Pain, and Rossella Arcucci. Generalised latent assimilation in heterogeneous reduced spaces with machine learning surrogate models. *Journal of Scientific Computing*, 94(1):11, 2023.
- [15] Zhao Ding, Chenguang Duan, Yuling Jiao, Jerry Zhijian Yang, Cheng Yuan, and Pingwen Zhang. Nonlinear assimilation with score-based sequential Langevin sampling. *arXiv preprint arXiv:2411.13443*, 2024.
- [16] Alessio Dore, Matteo Pinasco, and Carlo S. Regazzoni. Chapter 9 - multi-modal data fusion techniques and applications. In Hamid Aghajan and Andrea Cavallaro, editors, *Multi-Camera Networks*, pages 213–237. Academic Press, Oxford, 2009.
- [17] Geir Evensen. Sequential data assimilation with a nonlinear quasi-geostrophic model using monte carlo methods to forecast error statistics. *Journal of Geophysical Research: Oceans*, 99(C5):10143–10162, 1994.
- [18] Daniel Floryan and Michael D Graham. Data-driven discovery of intrinsic dynamics. *Nature Machine Intelligence*, 4(12):1113–1120, 2022.
- [19] Abhinav Prakash Gahlot, Rafael Orozco, Ziyi Yin, and Felix J Herrmann. An uncertainty-aware digital shadow for underground multimodal CO2 storage monitoring. *arXiv preprint arXiv:2410.01218*, 2024.

- [20] Jinwoo Go and Peng Chen. Sequential infinite-dimensional Bayesian optimal experimental design with derivative-informed latent attention neural operator. *arXiv preprint arXiv:2409.09141*, 2024.
- [21] S Hochreiter. Long short-term memory. *Neural Computation MIT-Press*, 1997.
- [22] Brian R Hunt, Eric J Kostelich, and Istvan Szunyogh. Efficient data assimilation for spatiotemporal chaos: A local ensemble transform kalman filter. *Physica D: Nonlinear Phenomena*, 230(1-2):112–126, 2007.
- [23] R. E. Kalman. A new approach to linear filtering and prediction problems. *Journal of Basic Engineering*, 82(1):35–45, 03 1960.
- [24] Diederik P Kingma and Max Welling. Auto-encoding variational Bayes. *International Conference on Learning Representations*, 2014.
- [25] Dmitrii Kochkov, Jamie A Smith, Ayya Alieva, Qing Wang, Michael P Brenner, and Stephan Hoyer. Machine learning–accelerated computational fluid dynamics. *Proceedings of the National Academy of Sciences*, 118(21):e2101784118, 2021.
- [26] Hans R. Künsch. Particle filters. *Bernoulli*, 19(4), September 2013.
- [27] Remi Lam, Alvaro Sanchez-Gonzalez, Matthew Willson, Peter Wirnsberger, Meire Fortunato, Ferran Alet, Suman Ravuri, Timo Ewalds, Zach Eaton-Rosen, Weihua Hu, et al. Learning skillful medium-range global weather forecasting. *Science*, 382(6677):1416–1421, 2023.
- [28] Zhuoyuan Li, Bin Dong, and Pingwen Zhang. Latent assimilation with implicit neural representations for unknown dynamics. *Journal of Computational Physics*, 506:112953, 2024.
- [29] Zhuoyuan Li, Bin Dong, and Pingwen Zhang. State-observation augmented diffusion model for nonlinear assimilation. *arXiv preprint arXiv:2407.21314*, 2024.
- [30] Lu Lu, Pengzhan Jin, Guofei Pang, Zhongqiang Zhang, and George Em Karniadakis. Learning nonlinear operators via DeepONet based on the universal approximation theorem of operators. *Nature machine intelligence*, 3(3):218–229, 2021.
- [31] Vivek Oommen, Khemraj Shukla, Somdatta Goswami, Rémi Dingreville, and George Em Karniadakis. Learning two-phase microstructure evolution using neural operators and autoencoder architectures. *npj Computational Materials*, 8(1):190, 2022.
- [32] Jaideep Pathak, Shashank Subramanian, Peter Harrington, Sanjeev Raja, Ashesh Chattopadhyay, Morteza Mardani, Thorsten Kurth, David Hall, Zongyi Li, Kamyar Azizzadenesheli, Pedram Hassanzadeh, Karthik Kashinath, and Animashree Anandkumar. FourCastNet: A global data-driven high-resolution weather model using adaptive Fourier neural operators, 2022.
- [33] Suraj Pawar and Omer San. Equation-free surrogate modeling of geophysical flows at the intersection of machine learning and data assimilation. *Journal of Advances in Modeling Earth Systems*, 14(11):e2022MS003170, 2022.
- [34] Stephen G Penny, Timothy A Smith, T-C Chen, Jason A Platt, H-Y Lin, Michael Goodliff, and Henry DI Abarbanel. Integrating recurrent neural networks with data assimilation for scalable data-driven state estimation. *Journal of Advances in Modeling Earth Systems*, 14(3):e2021MS002843, 2022.

- [35] Mathis Peyron, Anthony Fillion, Selime Gürol, Victor Marchais, Serge Gratton, Pierre Boudier, and Gael Goret. Latent space data assimilation by using deep learning. *Quarterly Journal of the Royal Meteorological Society*, 147(740):3759–3777, 2021.
- [36] Florence Rabier and Zhiqian Liu. Variational data assimilation: theory and overview. In *Proc. ECMWF Seminar on Recent Developments in Data Assimilation for Atmosphere and Ocean, Reading, UK, September 8–12*, pages 29–43, 2003.
- [37] Francesco Regazzoni, Stefano Pagani, Matteo Salvador, Luca Dede’, and Alfio Quarteroni. Learning the intrinsic dynamics of spatio-temporal processes through latent dynamics networks. *Nature Communications*, 15(1):1834, 2024.
- [38] François Rozet and Gilles Louppe. Score-based data assimilation. *Advances in Neural Information Processing Systems*, 36:40521–40541, 2023.
- [39] Samuel H Rudy, Steven L Brunton, Joshua L Proctor, and J Nathan Kutz. Data-driven discovery of partial differential equations. *Science advances*, 3(4):e1602614, 2017.
- [40] Matteo Salvador and Alison L Marsden. Liquid Fourier latent dynamics networks for fast GPU-based numerical simulations in computational cardiology. *arXiv preprint arXiv:2408.09818*, 2024.
- [41] D. Sanz-Alonso, A. Stuart, and A. Taeb. *Inverse Problems and Data Assimilation*. London Mathematical Society Student Texts. Cambridge University Press, 2023.
- [42] Rochelle Schneider, Massimo Bonavita, Alan Geer, Rossella Arcucci, Peter Dueben, Claudia Vitolo, Bertrand Le Saux, Begüm Demir, and Pierre-Philippe Mathieu. ESA-ECMWF report on recent progress and research directions in machine learning for earth system observation and prediction. *npj Climate and Atmospheric Science*, 5(1):51, 2022.
- [43] Phillip Si and Peng Chen. Latent-EnSF: A latent ensemble score filter for high-dimensional data assimilation with sparse observation data. *arXiv preprint arXiv:2409.00127*, 2024.
- [44] Yang Song, Jascha Sohl-Dickstein, Diederik P. Kingma, Abhishek Kumar, Stefano Ermon, and Ben Poole. Score-based generative modeling through stochastic differential equations, 2021.
- [45] Pantelis R Vlachas, Georgios Arampatzis, Caroline Uhler, and Petros Koumoutsakos. Multiscale simulations of complex systems by learning their effective dynamics. *Nature Machine Intelligence*, 4(4):359–366, 2022.
- [46] Junqi Yin, Siming Liang, Siyan Liu, Feng Bao, Hristo G Chipilski, Dan Lu, and Guannan Zhang. A scalable real-time data assimilation framework for predicting turbulent atmosphere dynamics. *arXiv preprint arXiv:2407.12168*, 2024.
- [47] Hao Zuo, Magdalena Alonso Balmaseda, Eric de Boisseson, Steffen Tietsche, Michael Mayer, and Patricia de Rosnay. The ORAP6 ocean and sea-ice reanalysis: description and evaluation. In *EGU General Assembly Conference Abstracts*, pages EGU21–9997, 2021.

A Training details

To determine the optimal hyperparameter choices for LDNets in our shallow water and Kolmogorov flow examples, we automate the hyperparameter search using Bayesian optimization [6]. The range of hyperparameters considered is listed in Table 2. The “downsample time steps” refers to the number of time steps sampled from the original dataset. Meanwhile, “ Δt normalize” is the constant used to normalize the time step Δt during the evolution of latent states. The details of further training and optimized hyperparameters are shown in Table 3. We also present the training parameters of LSTM encoder in Table 4.

Table 2: Hyperparameter search range for LDNets training

	Dataset	
	Shallow water	Kolmogorov flow
Downsampled time steps	20 – 50	20 – 50
Δt	0.03 – 0.05	0.04
Num of latent states	8 – 20	2 – 15
Dynamics net	depth	depth
	5 – 10	2 – 15
	width	width
	10 – 200	20 – 200
Reconstruction net	depth	depth
	5 – 10	2 – 15
	width	width
	100 – 250	20 – 700
StepLR (gamma)	0.1 – 0.8	0.1 – 0.9
Batch size	2 – 16	2 – 16

Table 3: Training details for LDNets

	Dataset	
	Shallow water	Kolmogorov flow
Downsample time step	50	40
Δt	0.036	0.04
Dynamics net	MLP	MLP
	8 hidden layers	9 hidden layers
	50 hidden dim	200 hidden dim
	ReLU	ReLU
Reconstruction net	MLP	MLP
	7 hidden layers	15 hidden layers
	180 hidden dim	500 hidden dim
	ReLU	ReLU
Initialization	Glorot normal	Glorot normal
Adam (lr)	10^{-3}	10^{-3}
StepLR (gamma, step size)	(0.6, 200)	(0.7, 200)
Batch size	2	6
Epoch	2000	2000
Loss	MSE	MSE

Table 4: Training details for LSTM encoder

	Dataset	
	Shallow water	Kolmogorov flow
Hidden layers	2	1
Hidden dim	256	128
Initialization	Glorot normal	Glorot normal
Adam (lr)	10^{-3}	10^{-4}
CosineAnnealingLR (Tmax, eta min)	(5000, 0.001)	(5000, 0.002)
Epoch	30000	30000
Dropout	0.02	0